17th World Conference on Earthquake Engineering, 17WCEE
Sendai, Japan - September 13th to 18th 2020

Simulation of the Surface Rupture following the 2016 Kumamoto Earthquake using High Performance Computing

M. Sawada[(1)], K. Haba[(2)], M. Hori[(3)]

[(1)] *Senior Research Scientist, Central Research Institute of Electric Power Industry, sawada@criepi.denken.or.jp*
[(2)] *Manager, Taisei Corporation, hb-kzm00@pub.taisei.co.jp*
[(3)] *Director-General, Japan Agency for Marine-earth Science and Technology, horimune@jamstec.go.jp*

Abstract

In the aftermath of the massive 1999 Taiwan and Turkey earthquakes, there has been a growing concern regarding potential damage to various infrastructures and buildings caused by surface fault ruptures. In this regard, for the on-site fault assessment of nuclear power plants, it is important to estimate the fault displacement. Important facilities were spared the primary faults that are a direct extension from earthquake source faults. Nevertheless, several cases of secondary faults beneath or close to these key facilities exist. Numerical simulation based on continuum mechanics has the potential to provide a reliable estimation of fault displacement.

However, there are major difficulties in numerical simulation of the fault rupture process. First, substantial numerical computations are required to simulate the fault rupture process even though the size of the target area is of the order of a few hundred meters. Second, the solutions of the initial and boundary value problem to which the numerical analysis is applied may suffer a loss of stability. Here, the stability loss implies drastic change in the solution induced by a small disturbance. We have developed a parallel finite element method wherein the following two functions are implemented: a symplectic time integration of the explicit scheme to properly conserve the energy of the fault, and rigorously formulated high-order joint elements.

We applied the numerical method to the simulation of the surface rupture in the 2016 Kumamoto earthquake. We constructed an analytical model of a 5 km × 5 km × 1 km domain including faults that appeared along the Kiyama river in Mashiki town. We categorized these faults into a primary fault that was the main rupture of Futagawa fault, and secondary faults distributed around the primary fault. We also modeled faults that were known to exist but did not appear in the 2016 earthquake as secondary faults. We applied forced displacements on the bottom surface of the analytical model based on the calculation of the elastic theory of dislocation using the slip distribution that was obtained by inversion analysis on the Futagawa and Hinagu faults. As the input slip increased, the surface slip appeared on both primary and secondary faults. Surface slips on secondary faults observed in the 2016 earthquake appeared prior to non-observed secondary faults. Furthermore, calculated surface slips agreed well with the measured values. Because the simulation reproduced the main features of the observed surface rupture, the proposed numerical method is applicable to surface fault displacement estimation.

We also conducted a predictive simulation using slip distributions on the primary fault that were set referenced to a strong ground motion prediction method for earthquakes with specified source faults. In this simulation, we obtained similar results to those from the simulation using slip distribution obtained by inversion analysis.

Keywords: fault displacement; surface rupture; high performance computing; joint element; parallel computing

1. Introduction

Since the occurrence of massive earthquakes in Taiwan and Turkey in 1999, there have been growing concerns regarding potential damage to various infrastructure and buildings caused by surface fault ruptures. For on-site fault assessment at nuclear power plants (NPPs), it is important to estimate fault displacements and their impact on facility safety functions. Important NPP facilities are separated from primary (or main) faults, which are direct extensions of earthquake source faults, by detailed geological surveys. However, there are several cases of secondary faults (or sub-faults) located beneath or close to important facilities. The activities of such sub-faults are being discussed.

Numerical simulations based on continuum mechanics are potential evaluation methods for surface fault displacements. However, major difficulties exist in simulating the fault rupture process. One challenge concerns the requirement of significant numerical computations to simulate the fault rupture process for a target area the size of which is only a few hundred meters. Another difficulty is the stability loss in the solutions of the initial and boundary value problem to which the numerical analysis is applied. Stability implies that a solution does not change when a small variation is added to the problem, and stability loss leads to drastic changes in the solution because of small disturbances. We overcame these difficulties by applying high performance computing methods. We developed a finite element method (FEM) involving two functions: 1) a symplectic time integration explicit scheme to properly conserve the energy of the system, and 2) rigorously formulated high-order joint elements. The FEM was enhanced with parallel computing capabilities [1, 2].

We applied this numerical method to the simulations of the 2014 Nagano-ken-hokubu earthquake wherein surface faulting was observed [3, 4]. The primary fault of this earthquake slipped as a reverse fault including a left-lateral strike-slip component. Through these simulations, we proposed a method of setting input fault slip distribution for predictive simulations [4].

Subsequently, we applied the numerical method to the simulation of the 2016 Kumamoto earthquake wherein the primary fault slipped as a right-lateral strike-slip fault including a normal slip component.

2. Numerical method

2.1 Estimation of fault displacement

For the fault displacement simulations, we constructed a continuum model of the ground and faults (see Fig. 1). An input slip Δ is given at the bottom of the primary (or main) fault and the surface slip δ is obtained after calculating the spread and dispersion of the slip on the fault plane. For on-site fault assessment at NPPs, surface slip on branch or secondary faults (or sub-faults) must be estimated rather than slip on the main fault.

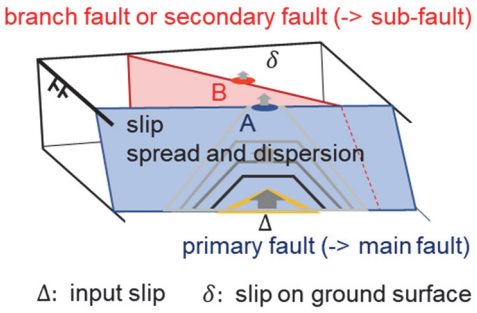

Fig. 1 – Spread and dispersion of a slip on faults

A fundamental difficulty in simulating the fault rupture process is stability loss in the solutions of the initial and boundary value problem, leading to significant changes in the solution because of small disturbances.

The treatment of uncertainties resulting from the limitations in the quality and quantity of the available relevant data for the underground structures, stress states, and source fault dynamics is important. Numerous simulations should be conducted under different conditions (capacity computing).

When considerable uncertainty exists, the surface fault displacement δ calculated by capacity computing is distributed over a wide range. In this case, δ is unpredictable in practice. It is important to evaluate the critical input slip Δ_c, which is the minimum input slip that causes surface slip, before evaluating δ. This idea is shown in Fig. 2.

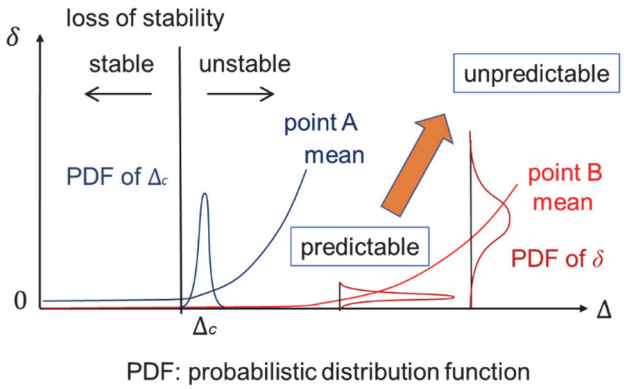

Fig. 2 – Evaluation of surface fault displacement

Quasi-static simulations allow determination of a relationship between the input and surface slips. This is extremely important for the estimation of Δ_c. Sawada et al. [2] showed the calculated Δ_c and δ in the quasi-static simulations were near those calculated in the dynamic simulations with damping, and proposed the use of quasi-static simulations for capacity computing. Hence, quasi-static simulations were also applied in this study.

2.2 FEM for the fault-displacement problem

We implemented a rigorous joint element for modeling slip behavior of faults and a symplectic time integration method with a Hamiltonian formulation in the open-source FEM program FrontISTR [5] to develop a numerical tool for fault displacement simulation.

In joint elements that are widely used in the field of rock mechanics, nodal forces are directly calculated from relative nodal displacements on a discontinuity [6]. Using this method, the element stiffness matrices are easily calculated. However, they differ from the standard method for constructing finite elements. Joint elements for fault-displacement simulations should be obtained to ensure proper convergence for the chosen element sizes and applicability to curved faults. We developed a rigorous joint element in which the element stiffness matrices were derived from the Lagrangian on the discontinuous surface using an isoparametric formulation [1].

We implemented the joint elements with a nonlinear spring-type constitutive equation to represent the fault movement. The following is the constitutive equation for shear movement of the joint element:

$$\tau = \kappa u, \tag{1}$$

where τ is the shear stress and u is the slip on the fault plane. The spring coefficient per unit area (shear stiffness) κ is described by the following function of the slip u:

$$\kappa(u) = \begin{cases} \kappa_0 - \frac{\kappa_0 - \kappa_d}{u_{cr}} u & (u \le u_{cr}) \\ \kappa_d & (u > u_{cr}) \end{cases}, \tag{2}$$

where κ_0 and κ_d are the initial and final shear stiffness, respectively, and u_{cr} is the critical slip (see Fig. 3). Notably, we did not use any sliders or dashpots in the model for κ.

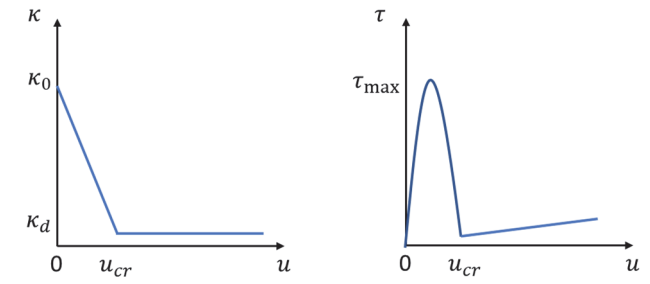

Fig. 3 – Nonlinear slip – shear stress relation

We considered the effect of the normal stress on the shear stiffness of the faults and defined the following equation:

$$\kappa_0 = \tilde{\kappa}_0(\sigma_n + b), \tag{3}$$

where $\tilde{\kappa}_0$ is the shear stiffness per unit normal stress, σ_n is the normal stress on the fault plane and b is a constant. We assumed the first peak of the slip–shear stress relation shown in Fig. 3 was identical to the shear strength. The parameters κ_0 and b in Eq. (3) can be determined such that the shear strength satisfied Coulomb's law of friction as follows:

$$\tilde{\kappa}_0 = \frac{4(1-\kappa_d/\kappa_0)}{u_{cr}} \tan\phi, \tag{4}$$

$$b = \frac{4c}{\tilde{\kappa}_0 u_{cr}} (1 - \kappa_d/\kappa_0), \tag{5}$$

where c is the cohesion and ϕ is the friction angle.

3. Simulation

3.1 The 2016 Kumamoto earthquake

The 2016 Kumamoto earthquake started with a Japan Meteorological Agency magnitude (M_{JMA}) 6.5 earthquake in the Kumamoto Prefecture, in the central part of Kyushu Island, southwest Japan, at 21:26 Japan Standard Time (JST) on April 14, 2016. A larger earthquake of M_{JMA} 7.3 occurred at 01:25 JST on April 16, 2016, just 28 hours later. A seismic intensity observation station at Mashiki town hall recorded a seismic intensity of 7 on the JMA scale during both events. The M_{JMA} 6.5 event on April 14 was the *foreshock*, and the M_{JMA} 7.3 event on April 16 was the *mainshock*. The mainshock was the simulation target in this study.

The earthquake occurred along the Futagawa and the northern Hinagu fault zones [7]. Surface faults 28 km and 6 km long were observed along the Futagawa and Hinagu fault zones, respectively (see Fig. 4). The north side of the Futagawa fault zone sank ≥ 1.0 m, and the south side rose ≥ 0.3 m. Horizontally, the northside of the Futagawa fault zone was displaced by more than 1.0 m to the east, and the south side was displaced by more than 0.5 m to the west. The surface faults were investigated, and the fault displacement distribution along them was obtained [8]. At Dozon in the eastern part of Mashiki town, a right-lateral strike-

slip fault of up to 2.2 m was observed. The surface fault branched out into two faults from Dozon to the west. Although these two branched-out faults exhibited a right-lateral strike-slip fault, a left-lateral strike-slip fault was observed between them. The target area of the numerical simulation is the 5 km × 5 km square area including those faults around Dozon as shown in Fig. 4.

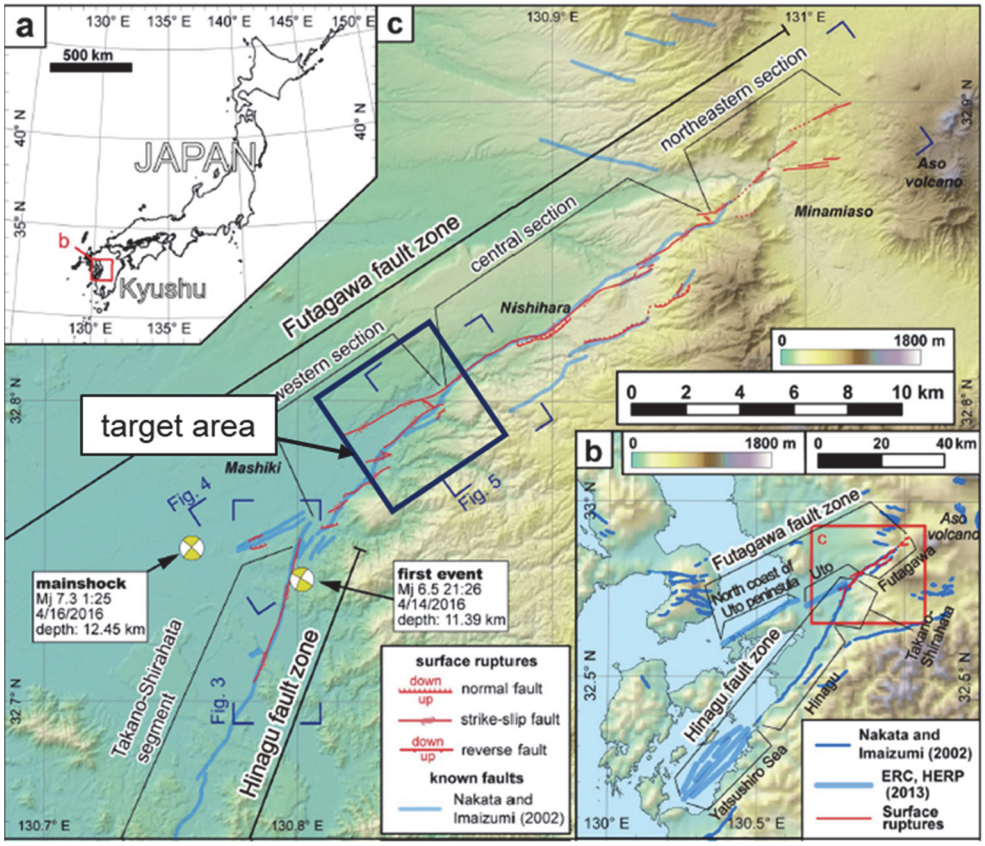

Fig. 4 – Map of the surface faults following the 2016 Kumamoto earthquake (modified; Shirahama et al. [8])

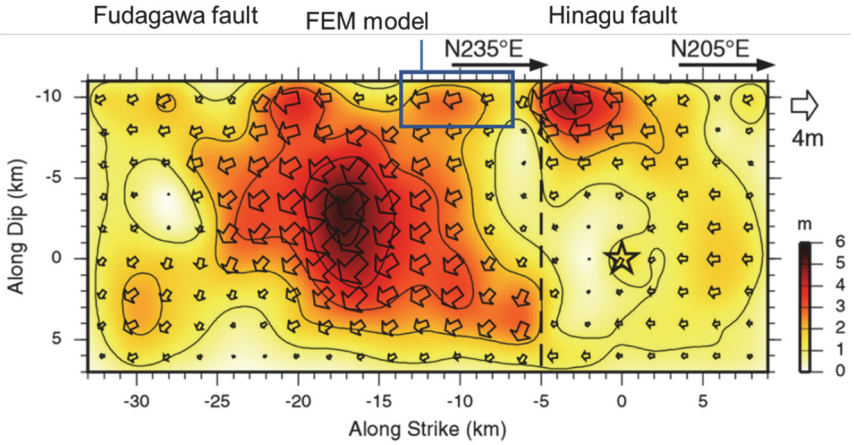

Fig. 5 – Slip distribution on main faults (modified; Asano & Iawata [9])

Asano and Iwata [9] conducted seismic source inversion analysis of the 2016 Kumamoto earthquake, and obtained slip distributions on the Futagawa fault and Hinagu fault as shown in Fig. 5. Futagawa fault and Hinagu fault slipped as right-lateral strike-slip faults including the normal fault component. The slip near the target area of the simulation was from 1.7 m to 2.6 m.

3.2 Analytical model

The target of the simulation is the 5 km × 5 km square area including branched-out faults in Mashiki town. The target depth from the ground surface is approximately 1 km. The National Research Institute for Earth Science and Disaster Resilience (NIED) provides a database on the crustal structure density and elastic wave velocity covering all of Japan on the web site of Japan Seismic Hazard Information Station (J-SHIS) [10]. In this database, elevational data regarding ground surface and boundaries of elastic wave velocity and density are given at the center of every node of 30” latitude and 45” longitude. We can construct an analytical model including the shape of the land and crustal structure using this database. We determined the strike and dip angles of the Futagawa fault and Hinagu fault in reference to Asano and Iwata [9]. The dip angles of Futagawa and Hinagu faults were 65°N and 72°N, respectively. Even though the upper edge of the faults did not reach the ground surface in their setting, we extended them to the ground surface with the same dip angle.

Fig. 6 shows the surface faults along the Kiyama river in Mashiki town, where the Futagawa fault branched out into two faults. We treated the line named *Main*, one of the two branched-out faults, as the main fault and is identical to the Futagawa fault. The other faults named *SubN* were included in the analytical model as sub-faults. Three faults named Sub2, Sub3, and Sub5 were observed in the 2016 earthquake, with Sub2 being the other branched-out fault. Sub3 was a left-lateral strike-slip fault bridging between Main and Sub2. Sub1 and Sub4 were faults known to exist before the 2016 earthquake; however, surface faulting was not observed along them in that earthquake.

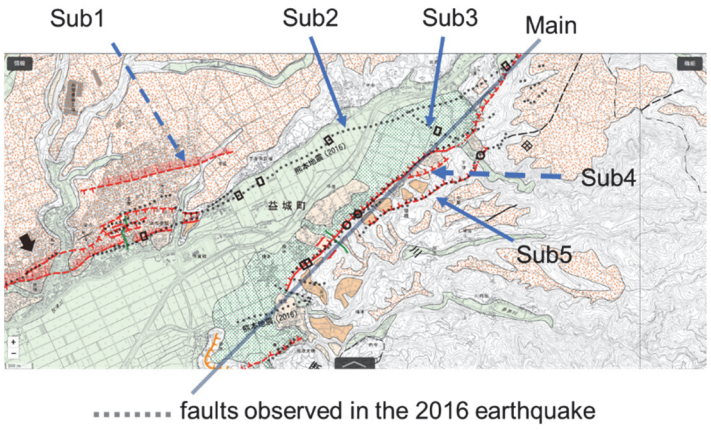

Fig. 6 – Surface faults along the Kiyama river in Mashiki town

Fig. 7 shows the finite element mesh of the analytical model. Faults were extended to the outer boundary or to the other faults. The Main, Sub4, and Sub5 strikes were parallel to the y-axis. The sub-fault dip angles were determined based on the results from the reflection seismic survey by Aoyagi [11]. Sub1, Sub2, and Sub4 were vertical. The ground was divided into three layers based on the J-SHIS database. The ground was discretized by second-order tetrahedral elements and the fault planes were discretized by second-order triangular joint elements. The fault plane element size was approximately 50 m and the total number of degrees of freedom was approximately 3.76 million. The white plots on a bird’s eye view in Fig. 7 indicate the location of output points for fault displacement results. *Y2780* means that the y-coordinate of these plots is 2780 m.

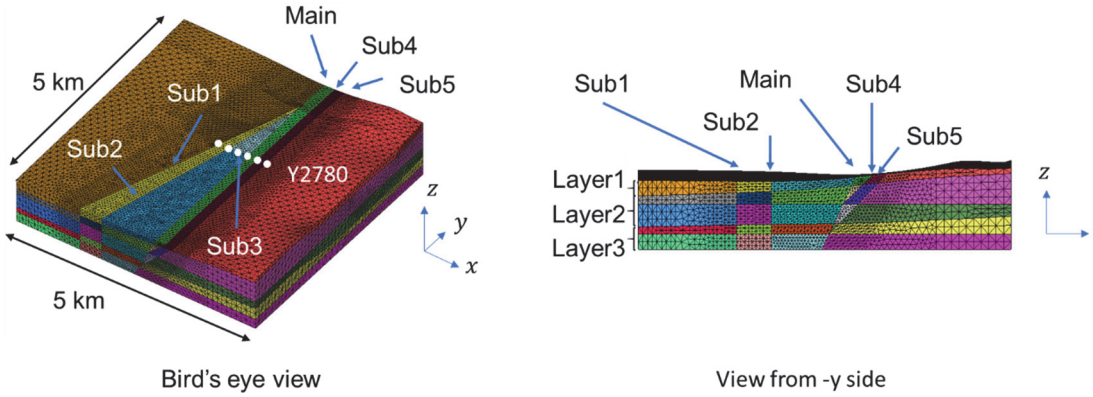

Fig. 7 – Finite element mesh

We assumed that the ground was a linear elastic body and determined Young's modules and Poisson's ratio of each layer from the density and the elastic wave velocity in the J-SHIS database. We conducted an initial stress analysis to determine the values of the parameters $\tilde{\kappa}_0$ and b on the fault planes from Eqs. (4) and (5) before the fault-displacement analysis. Normal displacements were fixed on the bottom and side boundaries in the initial stress analysis. We assumed a cohesion of 0.025 MPa and a friction angle of 25° on the fault planes. The ratio between the initial and final shear stiffness, κ_d/κ_0 was assumed to be 0.01 and the critical slip u_{cr} was 0.1 m. Material parameter values are summarized in Table 1.

Table 1 – Material parameters

	Young's Modulus (GPa)		**Poisson's Ratio**	**density (g/cm^3)**
Layer1	7.18		0.38	2.15
Layer2	27.7		0.31	2.40
Layer3	63.3		0.27	2.60
	friction angle (deg)	**cohesion (MPa)**	**shear stiffness ratio κ_d/κ_0**	**critical slip (m)**
faults	25	0.025	0.01	0.1

The size of the analytical model shown in Fig. 7 is smaller than the length of the main faults. The boundary conditions of the analytical model must be determined from a larger-scale analysis. We used the elastic theory of dislocations [12] with slip distribution on the main faults shown in Fig. 5 as the input. The upper edge of the faults was at a 2 km depth. We extended the faults to the ground surface and assumed that the slip on the extension was the same as the slip just below. We calculated ground displacement and determined the forced displacement at the bottom of the FEM model. The maximum slip on the bottom of the main fault was 5.2 m, which was twice the estimated 2.6 m slip. The other outer model boundaries were traction free. We termed this simulation *case1*.

3.3 Results

Fig. 8 shows the displacement norm contour and deformation of the analytical domain. The deformation is shown with 300-times amplification. When Δ was 2.6 m which was the estimated slip by Asano and Iwata [9], there was a displacement gap along Main, Sub2, and Sub5. In addition, there was a displacement gap along Sub1 and Sub4 when Δ was 5.2 m which was twice the estimated slip. This gap shows the surface slip on each fault.

Fig. 9 shows contour slip plots at Δ = 2.6 m on the main and sub-faults. There was a surface slip of greater than 1.0 m on the main fault and a surface of greater than 0.1m on Sub1, Sub2, and Sub5. The slipped area on Sub1 was limited compared to those on Sub2 and Sub5. The surface slips on Main, Sub2, and Sub5 were up to 1.25 m, 0.3 m, and 0.8 m, respectively. The sum of these values, 2.35 m was in good agreement with the sum of the observed slips [8]. The arrows in Fig. 9 point to Sub1, Sub2, and Sub5 contact edges with the main fault. The slipped sub-fault areas were propagated from the contact edges. In the 2014 Nagano-ken-hokubu earthquake simulation [3, 4], slip on the sub-fault was larger near the surface than near the contact edge with the main fault. The slip distribution on the sub-faults are remarkably different between the two earthquake simulations.

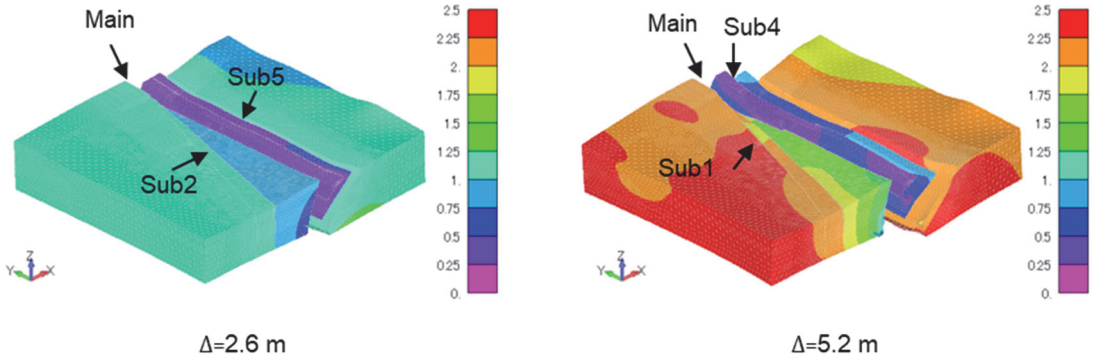

Fig. 8 – Contours of displacement norm and deformation (case1)

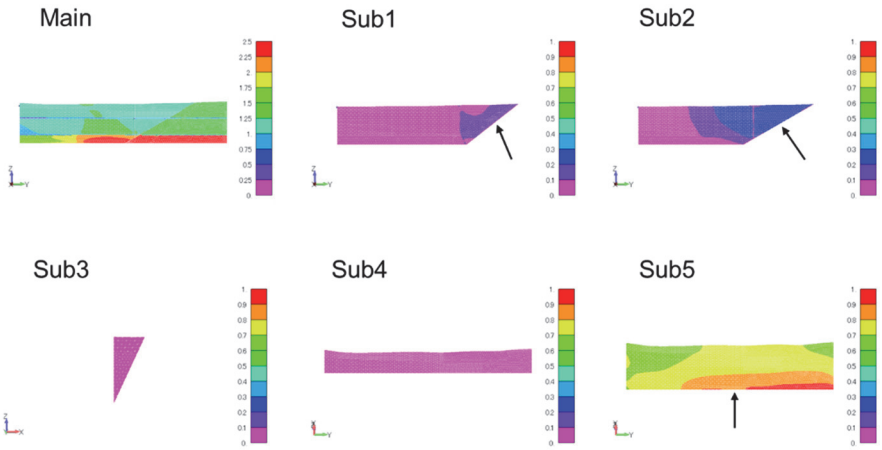

Fig. 9 – Contours of slip on the main fault and sub-faults (case1, Δ = 2.6 m)

Fig. 10 shows the variation in the surface net slip δ as the input slip Δ increases. There was a steep increase in the surface slip at Δ = 0.29 m on the main fault. A steep increase in the surface slip on the Sub5 and Sub4 began at Δ = 1.40 m and Δ = 3.04 m, respectively. Although there was no steep increase on Sub2, Sub1, or Sub3, the slip was more than 0.1 m at Δ = 1.22 m, Δ = 2.68 m, and Δ = 3.02 m, respectively. We defined Δ_c as the input slip at which surface slip exceeds 0.1 m and summarize the values of Δ_c at three locations on each fault in Table 2. The Δ_c was small on Sub2 and Sub5 where surface displacement was actually observed in the 2016 earthquake. The sense of slip on each location is also shown in Table 2. The sense of slip in the simulation was remarkably similar to that of observed surface faults.

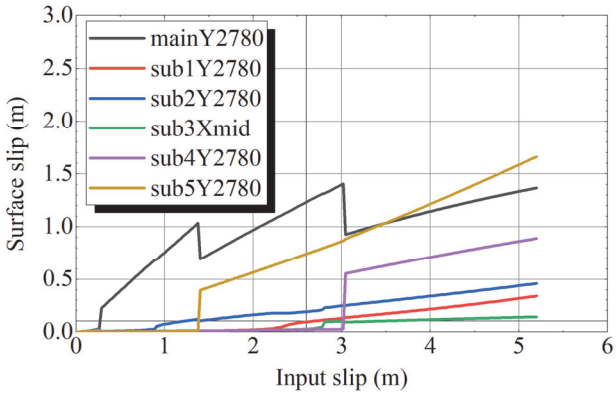

Fig. 10 – Surface slip – input slip relation (case1)

Table 2 – Slip sense and Δ_c on each fault (case1)

fault	Location*	observation	Δ_c (m)	simulation	
Main	1	right-lateral	0.29	right-lateral	east-up
	2		0.29	right-lateral	east-up
	3		0.29	right-lateral	east-up
Sub1	1	-	-	-	-
	2		2.68	right-lateral	east-up
	3		2.44	right-lateral	east-up
Sub2	1	right-lateral	1.69	right-lateral	east-up
	2		1.22	right-lateral	west-up
	3		0.91	right-lateral	west-up
Sub3	1	left-lateral south-up	4.32	-	south-up
	2		3.06	left-lateral	south-up
	3		2.83	left-lateral	south-up
Sub4	1	-	3.04	right-lateral	east-up
	2		3.04	right-lateral	east-up
	3		3.04	right-lateral	east-up
Sub5	1	east-up	1.40	right-lateral	east-up
	2		1.40	right-lateral	east-up
	3		1.40	right-lateral	east-up

* Location 1, 2 and 3 mean positoins of minimum, medium and maximum x-coordinate on Sub3, and positions of 1780 m, 2780 m and 3780 m y-coordinate on the other faults, respectively.

3.4 Predictive simulation

In predictive simulation, we are not able to use the results from seismic source inversion analyses like Fig. 5, and must assume the slip distribution on the main fault. We proposed the method to set the slip distribution and applied it to the simulation for the 2014 Nagano-ken-hokubu earthquake [4]. In this study, we applied the same method to the 2016 Kumamoto earthquake simulation. We set the slip distribution in reference to the strong motion prediction method termed *recipe* [13], which has the following steps: (1) set the main fault geometry (length, width, depth, and dip angle), (2) calculate the seismic moment, (3) calculate the average slip from the seismic moment and shear modulus of the crust, and (4) set the asperities number and location and calculate the slip on them and the other background. To calculate the seismic moment M_0, the following equation is used for relatively large earthquakes:

$$M_0 = \left(\frac{S}{4.24} \times 10^{11}\right)^2 \times 10^{-7}, \tag{6}$$

where S is the square of the main fault. We adopted the geometry of the Futagawa fault by Asano and Iwata[9]. As $S = 5.04 \times 10^8$ m^2 was derived from the length of 28 km and the width of 18 km, M_0 was calculated 1.41×10^{19} Nm. Average slip D was calculated from S and shear modules μ using the following equation:

$$D = M_0/(\mu \cdot S). \tag{7}$$

When we used μ = 30 GPa, $D = 0.934$ m was obtained. In this study, we did not set the asperities.

When we set only this average slip on the main fault, surface slip did not appear on the sub-faults. However, the slip along the surface fault was not generally uniform. Therefore, we set a large slip area on the main fault as shown in Fig. 11. We used the empirically obtained equation proposed by Matsuda et al. [14] to set the maximum surface slip:

$$D_{\max} = 10^{-4}L, \tag{8}$$

where $D_{\max}$ is the maximum surface slip and L is the surface rupture length. Here, we substituted 28 km of fault length to L and obtained $D_{\max} = 2.8$ m. In the simulation, maximum slip on the bottom of FEM model was 5.6 m, which was twice that of $D_{\max}$. We termed this simulation *case2*.

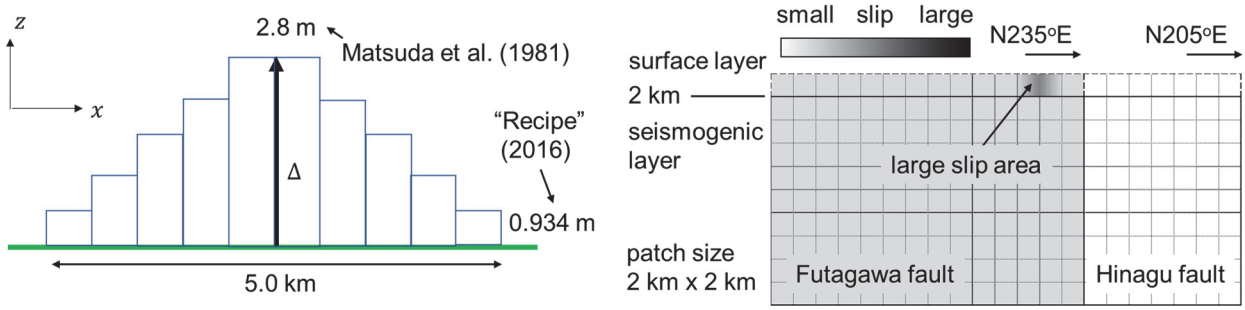

a) Slip distribution in large slip area

b) Slip distribution on the main faults

Fig. 11 – Setting slip distribution for predictive simulation

Fig. 12 shows the variation in the surface net slip δ as the input slip Δ increases. There was a steep increase in the surface slip at $\Delta = 0.36$ m on the main fault. The Δ_c on Sub1, Sub2, Sub3, Sub4, and Sub5 was 4.2 m, 2.7 m, 2.5 m, 3.1 m, and 1.6 m, respectively. On Sub2, Sub3, and Sub5 on which surface fault displacement was observed, Δ_c was less than 2.8 m. This tendency was similar to the case1 results. The surface slip was slightly smaller in case2 than in case1. Although the slip distributions at depth were significantly different between case1 and case2, the surface slip on the sub-faults were similar to each other.

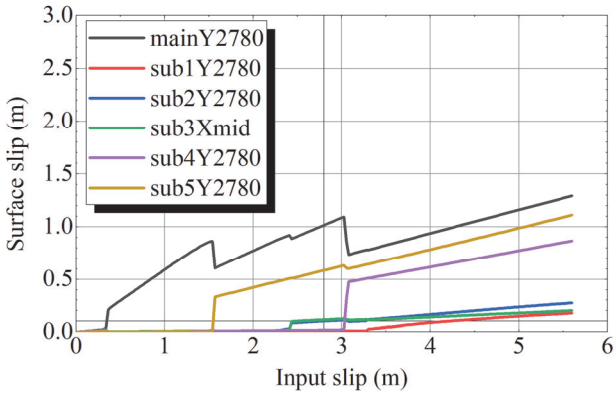

Fig. 12 – Surface slip – input slip relation (case2)

3.5 Discussion

We constructed a 5 km × 5 km × 1 km analytical model and derived the boundary conditions from the elastic theory of dislocation using slip distribution on the main fault obtained from a seismic source inversion analysis or using the strong motion prediction method and assuming a large slip area (predictive simulation).

When we provided the inversely analyzed slip on the main fault to the bottom of the analytical domain, we obtained a steep increase in surface slip on the main and sub-faults. On the sub-faults that actually appeared in the 2016 earthquake, the surface slip appeared at a smaller input slip than on the other sub-faults. The sense of the slip on each fault was remarkably similar to the observed sense. Furthermore, calculated surface slips agreed well with the measured values. Because the simulation reproduced the main features of the observed surface rupture, the proposed numerical method is applicable to surface fault displacement estimation.

However, some phenomena were not reproduced in the simulation. For example, the surface slip on Sub3 needed quite a large input slip. In the simulation, small faults tend to be less likely to slip.

In the predictive simulation, we obtained similar results to those of the simulation with the inversely analyzed input slip. We consider that the slip distribution on the main fault determined from the proposed method is for a case wherein surface slip on the sub-faults is likely to occur.

4. Conclusion

We developed a parallel FEM program to estimate surface fault displacement. In this study, we applied a numerical method to a 2016 Kumamoto earthquake simulation. We modeled a 5 km × 5 km × 1 km domain including branched-out faults and other sub-faults in Mashiki town. We applied the forced displacements on the model's bottom surface based on the slip distribution on the main faults and the elastic theory of dislocation. As the input slip increased, surface slip appeared on both the main and sub-faults. In the simulation, the surface slip appeared at a smaller input slip than on the sub-faults actually observed in the 2016 earthquake. The sense of the slip on each fault in the simulation was in good agreement with that observed in the earthquake. Furthermore, calculated surface slips agreed well with the measured values. We also applied the method to set the slip distribution on main faults as conditions under which surface slip on sub-faults is likely to occur for predictive simulation. This is the second application of the numerical method to real earthquakes. Because the simulations reproduced the main features of two different earthquakes, the numerical method is applicable to surface fault displacement estimation.

Acknowledgements

Dr. Aoyagi kindly provided us with information on the underground structure of faults in Mashiki town based on his results from the reflection seismic survey. We used the electric map for active faults in Kumamoto provided by Geospatial Information Authority of Japan on its the web site.

References

[1] Sawada M, Haba K, Hori M (2017): High performance computing for fault displacement simulation. *Journal of JSCE*, **73** (2), I_699-I_710. (in Japanese)

[2] Sawada M, Haba K, Hori M (2018): Estimation of surface fault displacement by high performance computing. *Journal of Earthquake & Tsunami*, **12** (4), 181003 (22 pages).

[3] Sawada M, Haba K, Hori M (2018): Evaluation of surface fault displacement in a real earthquake with surface faulting by high performance computing. *Journal of JSCE*, **74** (2), I_627-I_638. (in Japanese)

[4] Sawada M, Haba K, Hori M (2019): Simulation of the surface fault of the 2014 Nagano-ken-hokubu earthquake using high performance computing. *Transactions, SMiRT-25*, Charlotte, NC, USA.

[5] FrontISTR: https://www.frontistr.com, retrieved January 20, 2020.

[6] Goodman RE, Taylor RL, Brekke TL (1968): A model for the mechanics of jointed rocks, *Journal of ASCE*, **94** (SM3), 637-659.

[7] Fujiwara S, Yarai H, Kobayashi T, Morishita Y, Nakano T, Miyahara B, Nakai H, Miura Y, Ueshiba H, Kakiage Y, Une H (2016): Small-displacement linear surface ruptures of the 2016 Kumamoto earthquake sequence detected by ALOS-2 SAR interferometry. *Earth, Planets & Space*, **68**, DOI 10.1186/s40623-016-0534-x.

[8] Shirahama Y, Yoshimi M, Awata Y, Maruyama T, Azuma T, Miyashita Y, Mori H, Imanishi K, Takeda N, Ochi T, Otsubo M, Asahina D, Miyakawa A (2016): Characteristics of the surface ruptures associated with the 2016 Kumamoto earthquake sequence, central Kyushu, Japan. *Earth, Planets & Space*, **68**, DOI 10.1186/s40623-016-0559-1.

[9] Asano K, Iwata T (2016): Source rupture process of the foreshock and mainshock in the 2016 Kumamoto earthquake sequence estimated from the kinematic waveform inversion of strong motion data. *Earth, Planets & Space*, **68**, DOI 10.1186/s40623-016-0519-9.

[10] National Research Institute for Earth Science and Disaster Resilience: Japan Seismic Hazard Information Station (J-SHIS). http://www.j-shis.bosai.go.jp, retrieved January 20, 2020.

[11] Aoyagi Y (2018): Personal communication.

[12] Okada Y (1992): Internal deformation due to shear and tensile faults in a half-space, *Bulletin of the Seismological Society of America*, **82**, 1018-1040.

[13] The Headquarters for Earthquake Research Promotion (2016): Strong ground motion prediction method for earthquakes with specified source faults ("Recipe").

[14] Matsuda T, Yamazaki H, Nakata T, Imaizumi T (1981): The surface faults associated with the Rikuu earthquake of 1896. *Bulletin of Earthquake Research Institute, The University of Tokyo*, **55** (3), 795-855. (in Japanese)

